Fast, strong, and reversible adhesives with dynamic covalent bonds for potential use in wound dressing

Mingtao Chen[a], Yue Wu[b], Baohong Chen[a], Alexander M. Tucker[c], Anand Jagota[b], and Shu Yang[a,1]

Adhesives typically fall into two categories: those that have high but irreversible adhesion strength due to the formation of covalent bonds at the interface and are slow to deploy, and others that are fast to deploy and the adhesion is reversible but weak in strength due to formation of noncovalent bonds. Synergizing the advantages from both categories remains challenging but pivotal for the development of the next generation of wound dressing adhesives. Here, we report a fast and reversible adhesive consisting of dynamic boronic ester covalent bonds, formed between poly(vinyl alcohol) (PVA) and boric acid (BA) for potential use as a wound dressing adhesive. Mechanical testing shows that the adhesive film has strength in shear of 61 N/cm^2 and transcutaneous adhesive strength of 511 N/cm^2, generated within 2 min of application. Yet the film can be effortlessly debonded when exposed to excess water. The mechanical properties of PVA/BA adhesives are tunable by varying the cross-linking density. Within seconds of activation by water, the surface boronic ester bonds in the PVA/BA film undergo fast debonding and instant softening, leading to conformal contact with the adherends and reformation of the boronic ester bonds at the interface. Meanwhile, the bulk film remains dehydrated to offer efficient load transmission, which is important to achieve strong adhesion without delamination at the interface. Whether the substrate surface is smooth (e.g., glass) or rough (e.g., hairy mouse skin), PVA/BA adhesives demonstrate superior adhesion compared to the most widely used topical skin adhesive in clinical medicine, Dermabond.

hydrogel | dynamic covalent bonds | wound dressing | reversible | adhesives

Adhesion between two bodies is mediated by their surface or near-surface properties, including local chemistry or interfacial bonding that affects intrinsic adhesion at the molecular level, surface topography at the microscale, and the adherend materials' intrinsic mechanical properties. Covalent bonds such as those in superglue adhesives offer the strongest interactions (150 to 950 kJ/mol) (1) but require extended time (minutes to hours) or assistance by external stimuli (e.g., ultraviolet light and heat) to cure to achieve appreciable adhesion (2–5). Nevertheless, they are not reversible once cured. Adhesion based on molecular interactions, such as van der Waals forces (2 to 15 kJ/mol) and hydrogen bonds (10 to 40 kJ/mol) (1), could demand shorter time (seconds to minutes) to initiate adhesion and are reversible but the adhesion strength is usually much weaker (6–11). Typically, there are two trade-offs: 1) adhesion strength versus reversibility and 2) adhesion strength versus time required to activate adhesion and its evolution. For clinical use, an ideal wound dressing would reconcile both trade-offs for patients and doctors. Currently, wound closure relies either on sutures (or staples) or wound dressing adhesives (2). While sutures provide the strength needed for wound closure, they are time-consuming to place, are painful to patients, and require passing a needle through delicate skin edges. Wound dressing adhesives, on the other hand, are typically soft and noninvasive but also offer low adhesion force.

Various attempts have been made to address the two trade-offs. Nature-inspired surfaces with nano- or microstructured designs (e.g., gecko foot hair–inspired fibrillars) can achieve reversible adhesion (up to 50 to 70 N/cm^2) by accumulating noncovalent interactions, contact splitting, or interlocking (12, 13). However, it often requires sophisticated steps to fabricate these structures with a specific size, shape, and density or complementary surface textures. Our group has recently reported a hydrogel-based adhesive, demonstrating superglue-like adhesion strength (892 N/cm^2) and facile reversibility through noncovalent interactions via a shape adaptation mechanism (14). But it requires minutes to infuse water (for reversible release) and hours to dry the gel to achieve the ultrahigh adhesion, which is too slow for applications such as dressing wounds. Commercial wound dressing adhesives, such as Dermabond, achieve suitable adhesion in less than a couple of minutes through two-part cyanoacrylate chemistry, where acryl groups rapidly react with water (15). However, Dermabond adhesion is

Significance

It is challenging for wound dressing adhesives to realize both fast and strong adhesion yet be readily reversible, especially when the adherend skin surface is soft and hairy. By introducing boronic ester–based dynamic covalent bonds into polymer networks, we combine their covalent character to achieve strong adhesion and their dynamic nature for fast and reversible adhesion. Within seconds of water activation, the top surface of the adhesive film softens, allowing for conformal contact with the adherends. The bulk film remains dry and efficiently transmits the load within the network for strong adhesion. The incorporation of ultrafast and partially activated dynamic covalent bonds offers a concept for the next generation of wound dressing adhesives.

Author affiliations: [a]Department of Materials Science and Engineering, University of Pennsylvania, Philadelphia, PA 19104; [b]Departments of Chemical & Biomolecular Engineering and Bioengineering, Lehigh University, Bethlehem, PA 18015; and [c]Division of Neurosurgery, Children's Hospital of Philadelphia, Philadelphia, PA 19104

[1]To whom correspondence may be addressed. Email: shuyang@seas.upenn.edu.

not reversible due to the covalent cross-linking nature, and the resulting film is brittle and prone to fracture from the skin.

Dynamic covalent bonds that are capable of exchanging bond connectivity between multiple molecules offer opportunities to synergize strong covalent bond energy and dynamic bond exchange (similar to noncovalent bonds, such as hydrogen bonds) (16). Dynamic covalent bonds can be formed via transesterification (17–19), nucleophilic substitution (20–22), imine chemistry (23, 24), Diels-Alder reaction (25, 26), disulfide exchange (27, 28), thiol-X chemistry (29, 30), boronic esterification (31, 32), and silyl ether exchange (33, 34). Unzipping the bonds usually requires high temperatures, long reaction time (hours), use of catalysts/initiators, or external stimuli (16). Among them, boronic ester bonds obtained from reactions between diol-containing polymers such as polyvinyl alcohol (PVA) and boric acids (BAs) or boronic acids are an exception (16), because they undergo instantaneous (35) debonding and rebonding at ambient conditions without the use of catalysts or external stimuli. Researchers have utilized the dynamic nature of boronic ester bonds for controlled (supra)molecular assembly through competitive binding (36), demonstrating self-healing (37), and shape memory effect via pH fixation (38).

Mixtures of PVA and BA that are biocompatible and water soluble have been used as liquid adhesives (39, 40). BA reacts with the hydroxyl groups of PVA chains, forming boronic esters as the cross-link sites in the network, which are stable at alkaline conditions (at pH higher than the pK_a of BA, 9.2) but soluble in water at neutral pH (32). Compared to phenyl boronic acid that is commonly reported in the literature to react with vicinal diols (36), trifunctional BA is less sterically hindered. Therefore, it can react with nonvicinal -OH groups from adjacent polymer chains, including PVA (35), poly(tetramethylene ether glycol) (27), and poly(ethylene glycol) (37), leading to interchain cross-linking. However, cross-linked PVA/BAs are vulnerable to water for debonding, making it difficult to control their reversibility. As a result, literature on PVA/BA systems typically focuses on the covalent bond character of boronic esters and their applications as liquid adhesives. In order to achieve appreciable adhesion, these strategies require long adhering time (hours to days to evaporate water) (41, 42), whereas the instantaneous adhesion is weak (<0.1 N/cm^2) (43). Herein, we solution-cast PVA/BA aqueous solutions into dry films for potential application as wound dressing adhesives. As neutral pH favors the debonding of boronic ester bonds, PVA/BA is not cross-linked in solution. With the evaporation of water, BA is forced to react with both intra- and interchain -OH groups, causing intrachain folding and interchain cross-linking, respectively. For use, the dry PVA/BA film is activated by water submersion for a short period of time at neutral pH, which favors disassociation of the boronic ester bonds. Within seconds, the top surface is hydrated and softened while the bulk inner film remains dry and rigid (Fig. 1A). The softened film is compliant enough to make conformal contact with the adherend, whether it is smooth, rough, or rigid, upon pressing. Since the amount of water for evaporation on the surface is miniscule, when it is transported away from the film-substrate
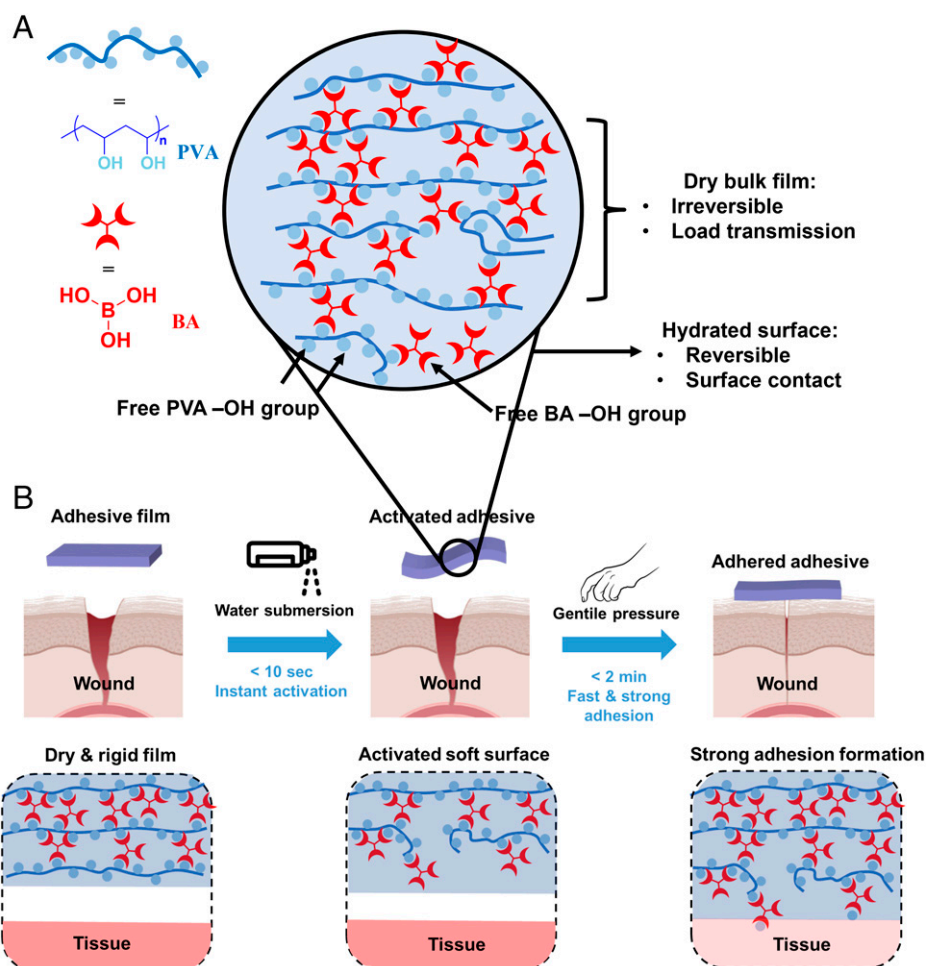

Fig. 1. Schematic illustrations of PVA/BA adhesives. (*A* and *B*) Instant softening of the top near-surface region upon water activation (*A*), allowing for fast adhesion to the wound site through dynamic covalent bonds (*B*).

interface into the bulk, covalent boronic ester bonds quickly reform within PVA/BA as well as between BA and the surface -OH group on the adherends, while the film remains conformal to the substrate (Fig. 1B). Additional hydrogen bonds between PVA and surface functional groups (such as -NH$_2$ and -OH) on the adherends also contribute to the adhesion. Meanwhile, the bulk film remains dry and retains film integrity such that the elastic chains between the cross-links offer an efficient pathway to transmit force. Therefore, the high modulus of the dry bulk film plays a critical role in achieving high adhesion strength in the dry state, while reducing the time for reversible adhesion.

Results and Discussion

Rheological Behaviors of PVA/BA Solutions. At neutral pH 7, the addition of BA into a PVA solution led to instant precipitation of a white gel (Movie S1). Fig. 2A depicts different physical appearances of PVA/BA hydrogels or solutions of different mixing ratios generated in neutral pH water. PVA/BA X/Y refers to the weight ratio between PVA (X) and BA (Y) while the total weight of PVA/BA in water is kept constant at 20 wt%. PVA/BA 2/1 and 3/1 that have high cross-linking densities form elastic gels that will not dissolve in water unless an excess amount of fresh water is added to initiate bond breakage, whereas
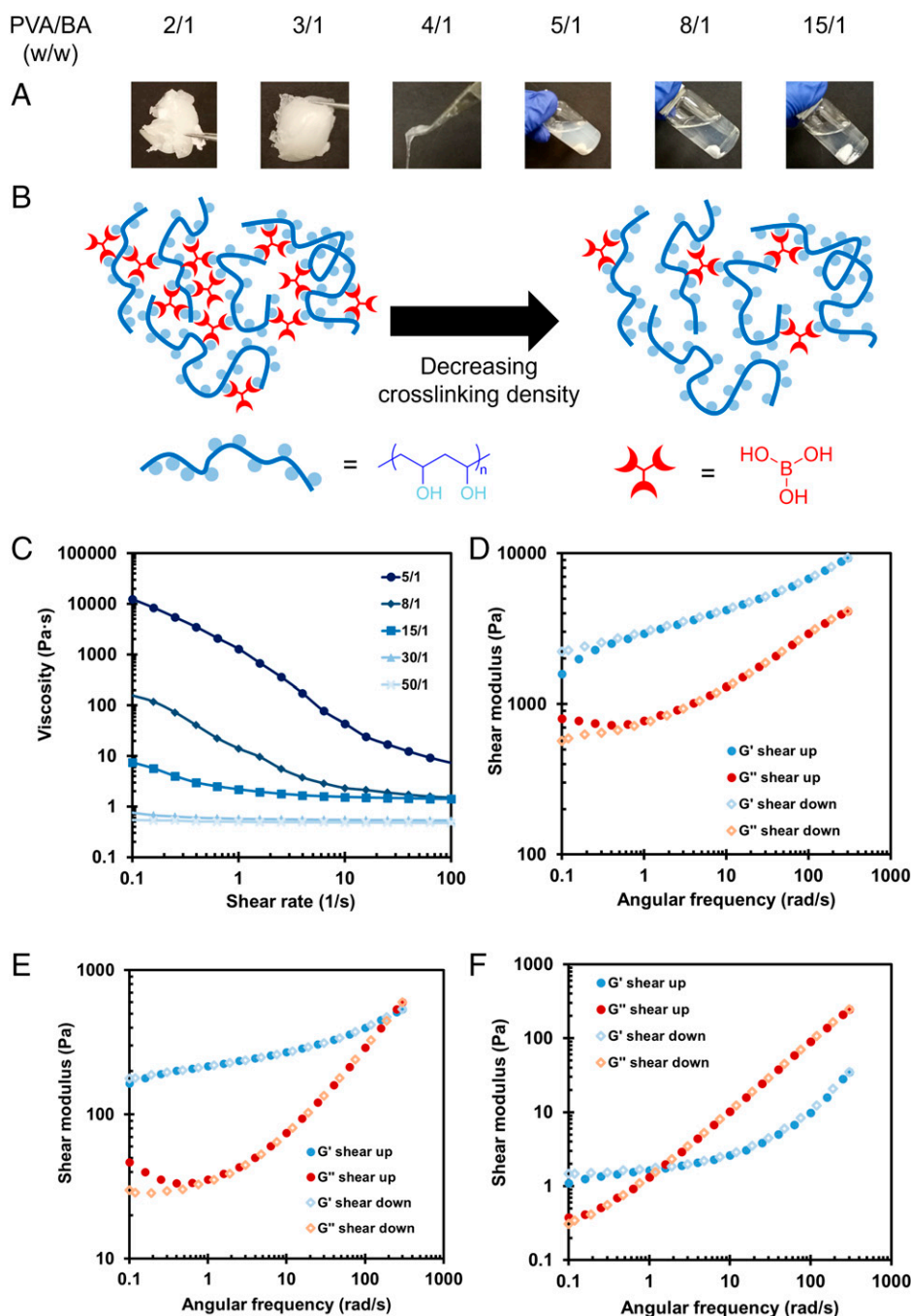

Fig. 2. Rheological behaviors of PVA/BA aqueous solutions in DI water (PVA/BA, 20 wt%). (A and B) Physical appearance of PVA/BA with different weight ratios (A) and corresponding illustrations of the network and chemical structures (B). (C) Shear sweep of PVA/BA 5/1, 8/1, 15/1, 30/1, and 50/1 solutions. (D–F) Frequency sweeps of PVA/BA 5/1 (D), 8/1 (E), and 15/1 (F) aqueous solutions. Filled blue circles denote the shear storage modulus (G') with increasing frequency; filled red circles, shear loss modulus (G") with increasing frequency; empty blue diamonds, shear storage modulus (G') with decreasing frequency; and empty red diamonds, shear loss modulus (G") with decreasing frequency.

Table 1. Summary of PVA/BA film mechanical properties

Composition	Young's modulus (MPa)	Ultimate modulus (MPa)	Strain at break	Toughness (MJ/m^3)
PVA/BA 5/1	913 ± 24	89.0 ± 5.3	0.15 ± 0.02	8.52 ± 1.84
PVA/BA 15/1	1,160 ± 139	85.3 ± 3.7	0.17 ± 0.02	10.23 ± 1.94
PVA/BA 30/1	761 ± 177	52.0 ± 7.4	1.29 ± 0.35	45.36 ± 8.77
PVA/BA 50/1	517 ± 147	33.1 ± 5.1	1.89 ± 0.25	54.16 ± 3.19

All values are reported as the mean (from at least three repeats) ± SD.

the initial gels formed in PVA/BA 5/1, 8/1, and 15/1 redissolve in water completely under constant stirring, forming a homogenous solution (Fig. 2B). The viscosity of the solution steadily decreased with decreasing cross-linking densities (from PVA/BA 5/1 to 50/1, Fig. 2C) according to a shear sweep measurement. All solutions demonstrated shear thinning, as the chains are aligned at high shear rates. The less cross-linked solution (PVA/BA 15/1) exhibited linear stress-shear rate response similar to that of ideal solutions, while the more cross-linked one (PVA/BA 5/1) demonstrated nonlinear stress response at a high shear rate (>1 rad/s) (*SI Appendix*, Fig. S1 *A* and *B*). To confirm the dynamic nature of the boronic ester bonds, a frequency sweep of PVA/BA solutions was conducted. The shear storage modulus (G') remained higher than the shear loss modulus (G") in PVA/BA 5/1 solution, indicating a solid-like behavior throughout the entire frequency range tested (Fig. 2D). Although the PVA/BA 5/1 solution flows easily at the ambient condition, the dynamic cross-links (boronic ester bonds) presented a solid-like stress response. Another important observation was that when the frequency was increased, the discrepancy between G' and G" diminished, which is counterintuitive for most polymer solutions or polymer melts. This is because at a high frequency (>10 Hz), most polymer solutions undergo incomplete relaxation. As a result, the materials behave more like a solid, leading to a large discrepancy between G' and G". Interestingly, in the PVA/BA 5/1 sample, a reverse trend was observed. In PVA/BA 8/1 (Fig. 2E) and PVA/BA 15/1 (Fig. 2F) solutions, the reverse trend continued to grow, and a cross-over between G' and G" occurred, indicating a transition from a solid-like behavior at low frequencies to a liquid-like behavior at high frequencies. This rare trend can be rationalized by the two orders of magnitude increase of the oscillation stress with increasing frequency (see *SI Appendix*, Fig. S1 *C* and *D*), which ruptured boronic ester bonds and weakened the matrix, leading to a liquid-like behavior. A repeated frequency sweep was conducted after each test (open symbols, shear down in Fig. 2D–F). Both G' and G" values overlapped with the first set of tests (filled symbols, shear up in Fig. 2D–F), indicating that water evaporation is negligible within the experimental duration.

As the cross-linking density is decreased, the modulus of the dry film is also reduced (*SI Appendix*, Fig. S2A) with good repeatability (*SI Appendix*, Fig. S2B). Meanwhile, the elongation strain at break is increased, showing increased toughness (see summary in Table 1). Since adhesion relies on interfacial contact, surface microroughness could significantly decrease the contact area. However, shaving hair, particularly on the head, in the operating room is time-consuming and a significant source of patient anxiety. Therefore, it is highly desirable to maintain good adhesion even on a hair-covered skin surface. Here, we test the adhesion strength of PVA/BA films on the smooth substrate, glass, and hairy mouse skin. Four common types of adhesion tests are reported in the literature, including lap shear, tensile, tack, and peeling tests (44). Here, we first applied indentation study to measure the adhesion strength after full

development as well as the underlying mechanism (Fig. 3). We then performed lap shear (Fig. 4A) and tensile tests (Fig. 4D) that are commonly applied to wound dressing adhesives. The adhesive strength is defined as the peak force divided by the contact area (length × width, for lap shear tests) or film cross-section (width × thickness, for tensile tests), respectively.

Indentation Study. To investigate the adhesion mechanisms of the PVA/BA system, we conducted indentation studies using a rigid glass sphere (diameter, 3.18 mm) sliding under a fixed normal load against a 0.4- to 0.5-mm-thick sample, PVA/BA 15/1. The samples were first dissolved in deionized (DI) water, transferred into 75-mm × 25-mm polydimethylsiloxane (PDMS) molds, and allowed to dry for 12 h at 30 °C, leaving a soft solid with a flat, smooth surface. From the central region of this sample, we cut out 10-mm × 10-mm pieces for sliding indentation experiments. These trimmed pieces were stuck onto 25-mm × 25-mm glass slides by softening the bottom surface. A custom-built sliding indentation setup was used to apply the vertical load through a load balance while a motorized linear stage (Newport) generated horizontal shear deformation (42), as shown in Fig. 3 *A* and *B*. The experiments were conducted at a sliding velocity of 1 μm/s. As described in previous sections, adhesion was activated by rehydrating parts of the sample surface. Here, the sample was rehydrated by applying a thin layer of water on the sample's upper surface for 30 s. As described previously, this softens a near-surface layer. The indenter was then placed on this softened surface with a fixed 49.03-mN load and allowed to dry for 10 h. During this process, the glass bead indented the sample, generating an approximately circular contact region and accompanying indent (see optical micrographs in Fig. 3). The indenter was then subjected to shear force, which was measured by the load cell.

Fig. 3 *C* shows typical shear force measured during such experiments. We note that the dried control sample was stiff and showed very low friction force. This is not surprising, as the indenter and the (dried and stiff) PVA/BA sample surface had minimal mutual contact. In the rehydrated samples, which formed a finite contact as shown in the inserted micrographs (Fig. 3C), the measured shear force increased dramatically as expected, with a maximum shear force ~70 times larger than that on the completely dried sample. The measured force increased continuously and linearly with the shear displacement (the load-drop near 0.8-mm displacement came from resetting of some backlash in the experimental setup). There was some indication of softening, which we associated with some subcritical reduction of the contact region. Complete indenter-sample detachment occurred at about 2-mm displacement, at a strong force of 5.85 ± 0.5 N. The scatter in this measurement was a result of variation in the actual contact region that, in turn, was due to inexact control of the water activation process. From the measured peak force, we extracted two quantities: 1) the maximum shear force per unit contact area, which corresponded to a hypothesis that separation occurred under a stress criterion; and 2) a critical stress intensity factor, which corresponded to
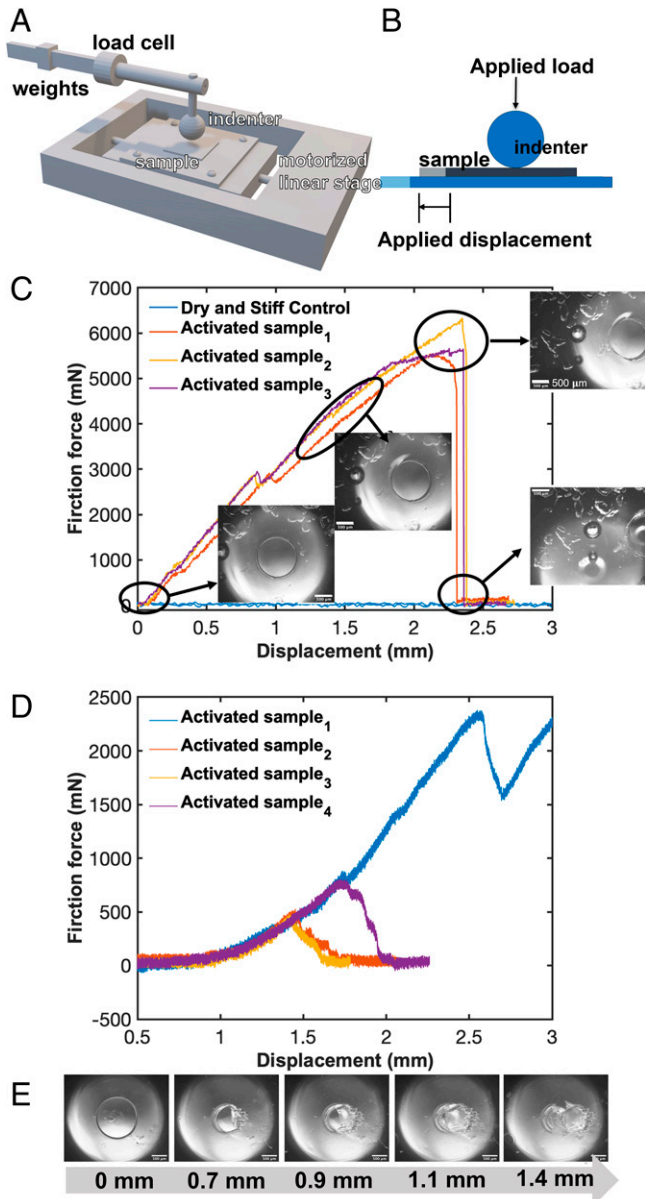
Fig. 3. (*A* and *B*) Schematic of the indentation (*A*) and shear (*B*) experimental setups. (*A*) Three-dimensional version of the main sliding mechanism. (*B*) Simplified side view of the shear indentation test. (*C*) Shear test on indented and dried PVA/BA (15/1). The indenter was brought into contact under a normal load of 49 mN after the sample had been rehydrated for 30 s. The shear load increases with displacement and releases abruptly at a critical shear load. (Scale bars, 500 μm in *Insets*.) (*D*) The indenter under a fixed normal load sheared with respect to the activated PVA/BA (15/1) samples. As the samples dry, the friction force increases. (*E*) Optical micrographs of the contact region suggest that it is lubricated to begin with. We usually observe a sinusoidal instability of the interface at the trailing edge of the contact (which is subject to normal tension). The force-displacement plots are consistent until failure, which is initiated at the defective trailing edge that shows significant sample-to-sample variation. (Scale bars, 100 μm.)

an assumption that separation was a fracture-controlled process. (The contact region diameter was measured by Fiji ImageJ.)

In order to quantify the results shown in Fig. 3*C* in the latter case, consider the approximate shear traction distribution in a circular contact region subjected to a shear load *T* as given in Johnson (Eq. **3.82** in ref. 45):

$$q_x(r) = q_0 \left(\frac{1}{\sqrt{1 - \frac{r^2}{a^2}}} \right) = \frac{T}{2\pi a^2 \left(1 - \frac{r^2}{a^2}\right)^{1/2}}, \quad [1]$$

where q_0 is the minimum shear traction (at the center of the circular contact), *a* is the contact radius, and *r* is the radial distance from the center of the contact. This can be rewritten as

$$q_x = \frac{T}{2\pi a^2} \frac{1}{\sqrt{1 - \frac{r^2}{a^2}}} = \frac{T}{2\pi a^2} \frac{a}{\sqrt{a^2 - r^2}}$$

$$= \frac{T}{2\pi a} \frac{1}{\sqrt{(a-r)(a+r)}}. \quad [2]$$

For $a \sim r$,

$$q_x \approx \frac{T}{2\pi a} \frac{1}{\sqrt{2a(a-r)}} = \frac{T}{\pi(2a)^{3/2}} \frac{1}{\sqrt{r'}}, \quad [3]$$

where $r' = a - r$.

Thus, the shear traction has a crack-like singularity at *r* = a and we can find the stress intensity factor, K_{II}, as

$$K_{II} = \sqrt{2\pi r'} \, q_x = \frac{T}{2\sqrt{\pi}a^{3/2}}. \quad [4]$$

The fracture toughness or the critical energy release rate of the interface is given by

$$G = \frac{K_{II}^2}{E}. \quad [5]$$

Taking the Young's modulus, *E*, of the completely dried PVA/BA sample to be ~1 GPa (Table 1), we can compute the fracture toughness *G*. In this manner, we find values of K_{II} of $1.66 \pm 0.31 \times 10^5$ N/m$^{3/2}$, *G* of 28.27 ± 9.88 J/m^2, and adhesion strength of 3.83 ± 0.52 MPa (383 N/cm^2), respectively.

In a second set of experiments, instead of applying displacement after the sample had dried completely, we initiated shearing displacement immediately after rehydrating the sample using the same experimental setup. That is, we measured the evolution of resistance to sliding as the PVA/BA sample dried. To improve load cell sensitivity, we reduced the applied normal load to 19.61 mN. Fig. 3*D* shows typical shear force measurements as a function of displacement/time. At the start of the experiment, the surface was hydrated and there was little friction. At a displacement of about 1 to 1.5 mm, which corresponded to drying time of about 1,000 to 1,500 s, we observed an increase in the friction, which corresponded to evaporation of water and formation of direct solid–solid contact representing the activation of adhesion. Shear force increased steadily and reached a local peak value, after which it fell as the contact was broken. The micrographs of the contact region (Fig. 3*E*) of the second test revealed that the contact region was hydrated at the start of the experiment. During sliding, we observed the formation of a fingering instability at the trailing edge of the contact. This coincided with the formation of solid–solid contact. Final shear separation of the indenter and sample initiated as an interfacial crack at the trailing edge, and the evident scatter in peak load (Fig. 3*E*) was due to experiment-to-experiment variability in the shape of the fingering instability.

The first experiment confirms that surface chemistry and near-surface shape adaptation work in concert to establish strong adhesion. The experiment also indicates that the contact adhesion breaks in a crack-like or fracture mode after the sample is completely dried and adhesion is developed. The second sliding indentation experiment, by converting the temporal evolution (which is difficult to observe) into a spatial evolution, reveals that the contact when wet is well lubricated, and it shows how onset of adhesion correlates with the formation of solid–solid contact along with a fingering instability at its trailing edge.
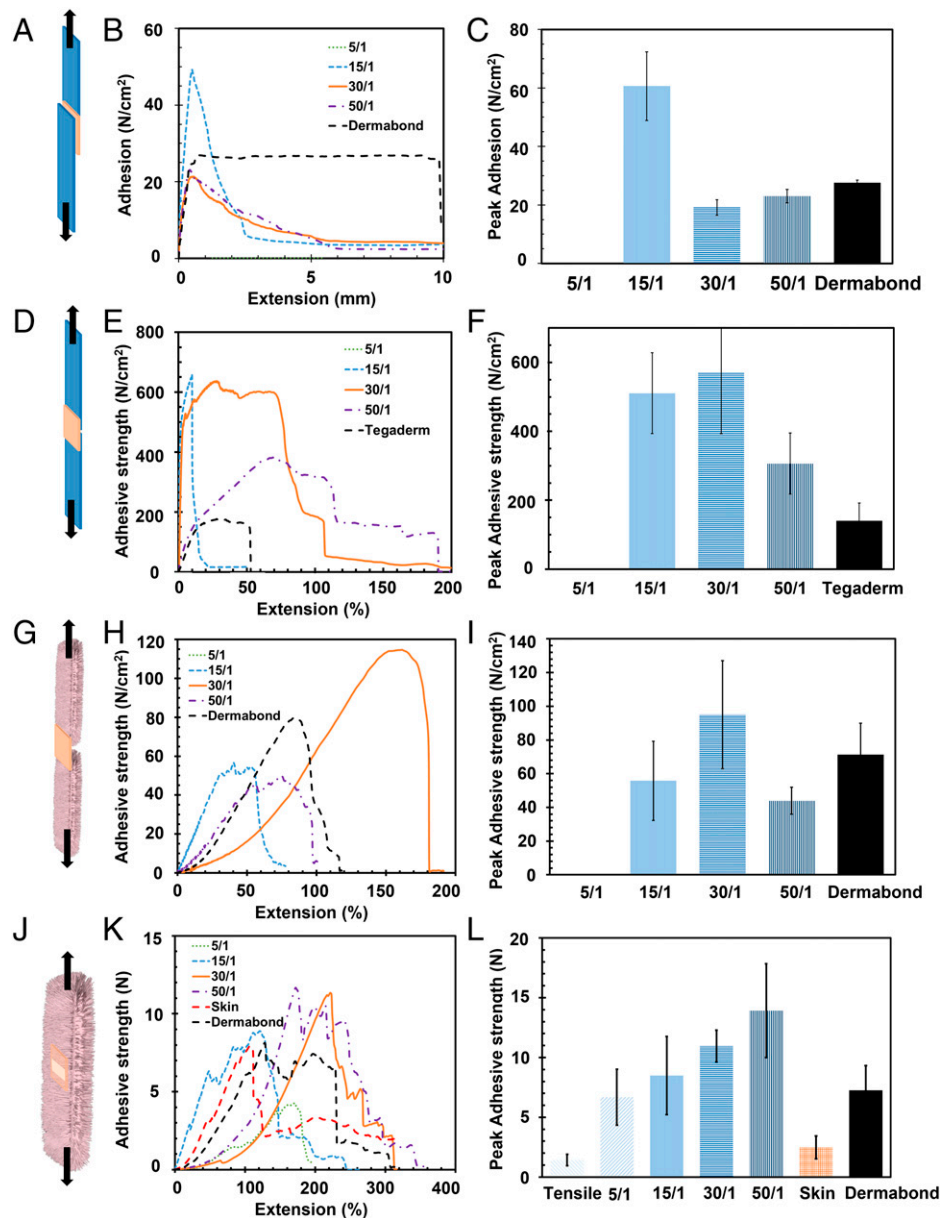
Fig. 4. (*A–F*) Adhesion performance of PVA/BA on glass. (*A*) Illustration of a single-joint lap shear test. (*B* and *C*) Representative single-joint lap shear test curves (*B*) and peak adhesion strength (*C*) of PVA/BA 5/1, 15/1, 30/1, and 50/1 films versus Dermabond. (*D*) Illustration of a tensile test to measure transcutaneous adhesive strength. (*E* and *F*) Representative tensile test curves (*E*) and peak adhesive strength (*F*) of PVA/BA 5/1, 15/1, 30/1, and 50/1 films versus Tegaderm. (*G–I*) Adhesive performance of PVA/BA adhesives on hairy mouse skins. (*G*) Illustration of a tensile test to study transcutaneous adhesive strength. (*H* and *I*) Representative tensile test curves (*H*) and peak adhesive strength (*I*) of PVA/BA 5/1, 15/1, 30/1, and 50/1 films versus Dermabond. (*J*) Illustration of an incision test to measure the adhesive strength around a skin cut. (*K* and *L*) Representative curves (*K*) and peak adhesive strength (*L*) of PVA/BA 5/1, 15/1, 30/1, and 50/1 films versus Dermabond and bare skin (with cut but no adhesives). All PVA/BA films were activated by dipping in water for 10 s, and 2-N force was applied on top to guarantee a good contact. Commercial products were applied as instructed with 2-N force on top for comparison.

Adhesion on Glass Substrates. PVA/BA films with various compositions were dipped in water for 10 s to activate the bond dissociation, and the films demonstrated strong shear and tensile adhesion after 2-min adhering time (with 2-N applied force on top). While the indentation study established that the interfacial separation of a dried contact proceeded in a fracture fashion, lap shear and tensile tests were closer to a real use scenario and provided direct comparison of our adhesion data with those from the literature.

In lap shear tests (Fig. 4*A*), all PVA/BA films showed a typical peak adhesion at the early stage of the experiments with cohesive failures (see representative stress-displacement curves in Fig. 4*B*). However, after 2 min, the liquid wound dressing adhesive, Dermabond, which was not fully cross-linked and

solidified, showed a plateau in force. PVA/BA 15/1 demonstrated the highest shear adhesion strength at 60.6 ± 11.7 N/cm^2 (Fig. 4*C*) after 2-min adhering time, doubling that of Dermabond, 27.6 ± 0.9 N/cm^2. Less cross-linked PVA/BA 30/1 and 50/1 exhibited lap shear adhesion strength, 19.1 ± 2.7 N/cm^2 and 23.0 ± 2.3 N/cm^2, respectively, similar to that of Dermabond. In contrast, PVA/BA 5/1 showed essentially no adhesion, as 10-s activation time was too short to soften the highly cross-linked surface layers. Previously reported wound adhesion strength is normally below 10 N/cm^2 within minutes of application for various adhesion tests (2, 46).

It is noted that the lap shear adhesion strength is sensitive to film thickness, hydration time, and adhering time. The lap shear adhesion strength of PVA/BA 15/1 films increased three

times when the film thickness was increased from 0.12 mm to 0.2 mm, from 18.7 ± 9.1 N/cm^2 to 60.6 ± 11.7 N/cm^2 (*SI Appendix*, Fig. S3*A*). At a fixed thickness (0.12 mm) of PVA/BA 15/1 film, the optimum hydration time is 6 s (31.6 ± 10.2 N/cm^2, *SI Appendix*, Fig. S3*B*). Shorter hydration time (4 s) leads to insufficient softening on the surfaces, lowering adhesion strength to 12.4 ± 5.6 N/cm^2, while longer hydration time (10 s or longer) deteriorated film integrity, also lowering adhesion strength to 18.7 ± 9.1 N/cm^2. Even PVA/BA 5/1 can be properly activated after 1-min hydration. Increasing adhering time can also alter the shear adhesion significantly. PVA/BA 15/1 started with adhesive strength of 16.4 ± 9.8 N/cm^2 after 30-s adhering time (*SI Appendix*, Fig. S3*C*), which slowly increased to 31.6 ± 10.2 N/cm^2 (2-min adhering time), then increased to 35.8 ± 15.6 N/cm^2 (10-min adhering time), and reached 106 ± 22 N/cm^2 after 30 min. In summary, PVA/BA is sensitive to water, so its mechanical properties and thus adhesive strength would change if exposed to different amounts of water. However, if the film retains its integrity, it can be dried for reuse (see the related discussion later). To prevent unwanted exposure to water, a hydrophobic backing layer could be added to the adhesive as seen in many commercial wound dressing films.

For wound dressing adhesives, another important characteristic is the transcutaneous adhesive strength—that is, the force provided by the adhesives to close the wound. We employed a tensile test to measure the transcutaneous adhesive strength, where a PVA/BA film was adhered to two glass slides from the same side, after which a uniaxial force was applied on both glass slides (Fig. 4*D*). PVA/BA 30/1 showed significantly longer extension at break (> 200%) than that of PVA/BA 15/1 (~50%, Fig. 4*E*). Among different films, PVA/BA 15/1 and 30/1 yielded the highest transcutaneous adhesive strength after 2-min adhering, 510 ± 117 N/cm^2 and 570 ± 177 N/cm^2, respectively (Fig. 4*F*), which is one to two orders of magnitude higher than literature values even after hours or days of development (3, 4). PVA/BA 50/1 showed a lower transcutaneous adhesive strength, 306 ± 89 N/cm^2, as a result of low cross-linking density and reduced film modulus. Its adhesion strength is still significantly higher than literature values or that of commercial wound dressing film, Tegaderm (2). We observed no adhesion from PVA/BA 5/1, as its shear adhesion is negligible. We note that in the transcutaneous adhesive tests, the adhesion performance relies on both the shear adhesion and the film elastic modulus. We note the surface -OH group density is not controlled in all studies (both on glasses and mouse skins) as we intended to mimic the real use conditions. Nevertheless, when the glass surfaces were treated with O$_2$ plasma to increase the surface density of -OH groups, the adhesive strength increased by almost an order of magnitude (*SI Appendix*, Fig. S3*D*). PVA/BA 15/1 film exhibited adhesive strength of 715 ± 76 N/cm^2 after 24-h developing time in a tensile test. A quick surface treatment of O$_2$ plasma further increased the adhesive strength to $5,803 \pm 1,410$ N/cm^2 (1-min O$_2$ plasma treatment) and $6,242 \pm 1,757$ N/cm^2 (3-min O$_2$ plasma treatment), demonstrating extremely strong bonding between PVA/BA film and -OH–rich surfaces. The relatively large SD in transcutaneous adhesive strength stemmed from the nonuniformity of the O2 plasma treatment and errors of film-thickness measurement (~0.2 mm) by a caliper. Nevertheless, the effect of OH groups on surface is obvious.

At neutral pH, debonding is favored. Thus, overexposure in water should weaken PVA/BA film adhesion significantly. *SI Appendix*, Fig. S3*E* shows that after 30-s submersion in water, PVA/BA adhesive films could be easily peeled off from glass,

where the transcutaneous adhesive strength dropped from 570 ± 177 N/cm^2 to 49 ± 23 N/cm^2. This weakened adhesive film could be easily removed from the substrates and reapplied on glass slides. Within 2 min of water evaporation, the adhesive strength increased back to 330 N/cm^2 again, demonstrating their promising potential as strong and reversible adhesives that are reusable. However, after 2-h submersion in water, PVA/BA films were completely dissolved.

Adhesion Tests on Mouse Skin. It would be highly advantageous if the adhesive could work on actual skin without the need to remove hair prior to surgery. For example, head wound sites are notoriously challenging to close with skin adhesive or bandages. Cranial surgical wounds are traditionally closed with suture, which requires thorough hair shaving around the incision site that can be extremely distressing to patients. Closed wounds are typically dressed in gauze covering the head, which are difficult to place, uncomfortable to wear, and do not affect wound healing. Bulky dressings can elicit anxiety in patients, particularly children, and tight headwraps can be painful. Current tissue adhesives either cannot provide strong enough adhesion or lack facile removal options. Common removal strategies include waiting for the adhesive to fall off, which could take weeks, pulling it off the hair, which can be extremely painful for children who have delicate skin, or cutting it out of the involved hair once the wound is healed.

PVA/BA dynamic bonds offer a potential solution to balance reversibility and adhesion strength. To quantitatively analyze the adhesion performance of PVA/BA films as wound dressing adhesives on unshaved, hairy surfaces, we employed hair-covered mouse skins as adherends. PVA/BA adhered to mouse skins with both higher transcutaneous (Fig. 4*G*) and incision (Fig. 4*J*) adhesive strength compared with those of Dermabond. Transcutaneous adhesive strength was determined through tensile tests described earlier, while incision adhesion was tested through a revised tensile test procedure: instead of two separate mouse skins, an incision (1-cm wide) was introduced at the middle of one intact skin (2-cm wide). The film was then applied on top of the incision for 2 min.

Due to the complexity of mouse skin, both PVA/BA and Dermabond recorded lower transcutaneous adhesive strength than that on glass. In the representative stress-strain curves (Fig. 4*H*), PVA/BA 30/1 exhibited the longest extension due to its low cross-linking density. PVA/BA 15/1 had a significant mismatch of the Young's modulus between the dry adhesive film (1.2 GPa) and the much softer mouse skin (25 to 260 kPa), deteriorating the shear adhesion at the interface. The less cross-linked PVA/BA 50/1 shows better shear adhesion, but its inferior tensile properties lead to a lower transcutaneous adhesive strength. In terms of peak adhesive strength, PVA/BA 30/1 still demonstrated strong adhesion, 95 ± 32 N/cm^2 (Fig. 4*I*), after 2 min, whereas most literature studies reported less than 30 N/cm^2 tensile adhesion after hours of adhering (2). Dermabond showed a slightly lower adhesive strength of 71.3 ± 18.6 N/cm^2 that we attribute to its liquid nature, which allows it to go in between hairs on mouse skins for further cross-linking. PVA/BA 15/1 and 50/1 also showed promising adhesion, 55.8 ± 23.6 N/cm^2 and 43.9 ± 8.0 N/cm^2, respectively. PVA/BA 5/1 remained inactivated after 10-s hydration time.

In surgical wounds, the skin beyond the wound margin remains connected. Hence, to better understand adhesion similar to those found in surgical wounds, we employed an incision test (Fig. 4*J*) to measure PVA/BA's adhesive strength on hairy mouse skin. Due to its liquid nature, we could not accurately

measure Dermabond's thickness. Hence, we measured the peak force (Fig. 4 *K* and *L*) instead of peak pressure as a function of extension. As the skin contributes partially to the tensile properties, a good contact at the interface between the adhesive and the adherend is pivotal to generate strong adhesion. PVA/BA 50/1 that has the lowest cross-linking density and thus lowest modulus provides the best contact with the skins. Fig. 4*K* depicts representative force-strain curves during the incision tests. The peak adhesion of high-modulus adhesives (PVA/BA 5/1, 15/1, and Dermabond) coincided with that of the bare mouse skin used as the control (at ~100% strain), where poor interfacial contact led to adhesive failures (*SI Appendix*, Fig. S4A). Conversely, softer adhesives (PVA/BA 30/1 and 50/1) benefited from better contact with the hairy skin and peaked at longer extension (>200% strain) with cohesive failures (*SI Appendix*, Fig. S4B). As a result, PVA/BA 50/1 exhibited the strongest adhesion force at 13.9 ± 3.9 N (or $1,159 \pm 327$ N/cm^2), roughly twice of the Dermabond adhesion (7.3 ± 2.0 N) (Fig. 4*L*). With the increased cross-linking density, the adhesion force decreased from 11.0 ± 1.3 N (PVA/BA 30/1) to 6.7 ± 2.3 N (PVA/BA 5/1). PVA/BA incision tests demonstrated synergistic adhesion as the summed adhesion force of the bare skin (with incision but no adhesives, labeled as "skin" in Fig. 4*L*) and tensile tests (labeled as "tensile" in Fig. 4*L*) fell short to the PVA/BA incision adhesion force ("30/1" in Fig. 4*K*).

Preliminary translational adhesive work on in situ mouse skin has reported conclusions similar to the above transcutaneous adhesion tests and incision tests. All films were dipped in water for 10 s and applied to the mouse skin immediately for 2 min before testing. PVA/BA 15/1 (Movie S2) showed good adhesion across the wound site but lacked conformability to the soft skin. PVA/BA 30/1 (Movie S3) exhibited excellent adhesion and enough flexibility to conform and tightly adhere to the soft mouse skin. Its adhesion persisted until the mouse skin started to rupture after pulling apart with forceps. Further decrease of the cross-linking density to 50/1 reduced the film integrity, which was easily separated from the mouse skin upon pulling (Movie S4).

In summary, we successfully prepared PVA/BA films with dynamic covalent bonds as potential wound dressing adhesives that outperform a widely used cyanoacrylate-based commercial product, Dermabond, while achieving fast and reversible adhesion. Partial hydration of the top surface of PVA/BA films allows for instant softening and thus fast debonding at the interface. Meanwhile, the dry bulk film retains high Young's modulus (500 to 1,000 MPa depending on cross-linking density) to transmit load efficiently. Synergistically, the PVA/BA films demonstrate superior transcutaneous adhesive strength on both smooth substrate glass (570 ± 177 N/cm^2) and hairy mouse skin (95 ± 32 N/cm^2) compared to those of Dermabond (140 ± 52 N/cm^2 on glass and 71.3 ± 18.6 N/cm^2 on mouse skin). PVA/BA adhesives achieve orders of magnitude stronger and faster adhesion, while they can be removed effortlessly upon wetting compared to previously reported wound adhesives (2, 3, 5). Therefore, PVA/BA is a promising replacement of current wound dressing adhesives without complex engineering and fabrication processes, while offering multiuse options. Further, the rich boronic ester chemistry will allow us to tailor PVA/BA formulations for specific needs. For example, our preliminary study suggests that the addition of hydrophobic phenyl BA can significantly improve the water repellency of PVA/BA adhesives while maintaining other advantages.

Materials and Methods

Materials. PA (molecular weight, 13,000 to 23,000 g/mol; 87 to 89% hydrolyzed) was purchased from Sigma-Aldrich and used without further treatment. BA (DNase, RNase, and protease free, 99.5%) was purchased from Acros Organics and used directly. Mouse skins were freshly provided by the Children's Hospital of Philadelphia and cut into rectangular shapes before tests. Commercial adhesive products, Dermabond (Ethicon) and Tegaderm (3M), were purchased from corresponding vendors and used as instructed by the user manual.

PVA/BA Solution. PVA was dissolved in DI water first to form a homogeneous solution. With vigorous stirring, BA solids were charged into the solution directly. White precipitates appeared instantly. Continuous stirring redissolved the precipitates to yield a homogeneous solution again at room temperature. The total weight ratio of PVA and BA in water was kept at 20 wt%. Take the preparation of PVA/BA 15/1 solution as an example: First, PVA (2.34 g) was dissolved in DI water (10 g) overnight. BA (0.16 g) was then added into the PVA solution directly with vigorous stirring with instant white precipitates formed. The solution was stirred for another 24 h to redissolve the white precipitates until a homogenous solution was formed.

PVA/BA Film Preparation. The PVA/BA aqueous solution (20 w%) was casted on glass substrates using a doctor blade to maintain a uniform thickness (2 mm). The casted solution was left to dry at ambient conditions for 48 h with a glass cover to prevent dust. The dried films were peeled off from the glass substrates directly before use.

Rheological Measurements. All rheological measurements were conducted on a Discovery Hybrid Rheometer HR 20 with a 40-mm 0.998333° cone plate (UHP Steel). The gap was kept at 1,000 μm, and the temperature was maintained at 25 °C.

The shear sweep was performed from 0.1 to 100 s^{-1}. The strain sweep was conducted from 0.01 to 50% at 1 Hz. The frequency sweep was conducted from 0.1 to 300 rad/s first and from 300 to 0.1 rad/s second at 1% strain.

Adhesion Tests. Most adhesion tests were performed on an Instron machine (5564 Tabletop Materials Testing System) in tensile mode at a 5-mm/min rate and room temperature. Each test was repeated at least three times and reported as the average value with SD.

Sample preparation. PVA/BA films were cut into rectangular shapes (10 × 10 × 0.02 mm) before hydration in DI water for 10 s. For lap shear tests, both sides were hydrated, while only one side was wetted for tensile and incision tests. The activated adhesives were adhered to untreated substrates (glass or mouse skin) with 200-g weight on top to guarantee good contact. The entire sample was placed on a hot plate at 37 °C to mimic the body temperature and developed for 2 min before adhesion tests. For liquid adhesives, Scotch tape was used to confine the adhesive areas of Dermabond. In incision tests, the mouse skin was cut into 2 × 4 cm, followed by a 1-cm incision in the middle of the skin.

For reversibility tests, the samples were prepared in a way similar to that for tensile tests. After 2-min adhering time, the tensile samples were submerged into DI water for an additional 30 s before they were subjected to adhesion tests. For surface-treated glasses, the substrates were subjected to O$_2$ plasma cleaning (Harrick PDC-001 and PlasmaFlo PDC-FMG) with airflow at a high radial frequency (RF) level (30 W).

Adhesion data. The adhesion strength in lap shear tests was calculated using peak force divided by the adhesive contact area (length × width). In tensile tests, the adhesion was reported as peak force divided by the film cross-sectional area (width × thickness). In incision tests, peak force was directly utilized to represent adhesion. Each test is repeated at least three times and reported as the average value with SD.

Data Availability. All study data are included in the article and/or supporting information.

1. A. J. Kinloch, The science of adhesion. *J. Mater. Sci.* **15**, 2141–2166 (1980).
2. Y. Gao *et al.*, Hydrogel-mesh composite for wound closure. *Proc. Natl. Acad. Sci. U.S.A.* **118**, e2103457118 (2021).
3. C. L. Jenkins, H. M. Siebert, J. J. Wilker, Integrating Mussel chemistry into a bio-based polymer to create degradable adhesives. *Macromolecules* **50**, 561–568 (2017).
4. J. Li *et al.*, Tough adhesives for diverse wet surfaces. *Science* **357**, 378–381 (2017).
5. E. Shirzaei Sani *et al.*, Sutureless repair of corneal injuries using naturally derived bioadhesive hydrogels. *Sci. Adv.* **5**, eaav1281 (2019).
6. E. Arzt, S. Gorb, R. Spolenak, From micro to nano contacts in biological attachment devices. *Proc. Natl. Acad. Sci. U.S.A.* **100**, 10603–10606 (2003).
7. L. Han, M. Wang, L. O. Prieto-López, X. Deng, J. Cui, Self-hydrophobization in a dynamic hydrogel for creating nonspecific repeatable underwater adhesion. *Adv. Funct. Mater.* **30**, 1907064 (2020).
8. R. Hensel, K. Moh, E. Arzt, Engineering micropatterned dry adhesives: From contact theory to handling applications. *Adv. Funct. Mater.* **28**, 1800865 (2018).
9. J.-K. Kim, M. Varenberg, Drawing-based manufacturing of shear-activated reversible adhesives. *ACS Appl. Mater. Interfaces* **12**, 20075–20083 (2020).
10. S. Rose *et al.*, Nanoparticle solutions as adhesives for gels and biological tissues. *Nature* **505**, 382–385 (2014).
11. Y. Wang *et al.*, Instant, tough, noncovalent adhesion. *ACS Appl. Mater. Interfaces* **11**, 40749–40757 (2019).
12. C.-M. Chen, C.-L. Chiang, C.-L. Lai, T. Xie, S. Yang, Buckling-based strong dry adhesives via interlocking. *Adv. Funct. Mater.* **23**, 3813–3823 (2013).
13. Y. Rahmawan, S. M. Kang, S. Y. Lee, K.-Y. Suh, S. Yang, Enhanced shear adhesion by mechanical interlocking of dual-scaled elastomeric micropillars with embedded silica particles. *Macromol. React. Eng.* **7**, 616–623 (2013).
14. H. Cho *et al.*, Intrinsically reversible superglues via shape adaptation inspired by snail epiphragm. *Proc. Natl. Acad. Sci. U.S.A.* **116**, 13774–13779 (2019).
15. Ethicon, Dermabond skin closure system. https://www.jnjmedtech.com/en-US/product/dermabond-advanced-topical-skin-adhesive. Accessed 8 July 2022.
16. P. Chakma, D. Konkolewicz, Dynamic covalent bonds in polymeric materials. *Angew. Chem. Int. Ed. Engl.* **58**, 9682–9695 (2019).
17. D. Montarnal, M. Capelot, F. Tournilhac, L. Leibler, Silica-like malleable materials from permanent organic networks. *Science* **334**, 965–968 (2011).
18. Y. Yang, Z. Pei, Z. Li, Y. Wei, Y. Ji, Making and remaking dynamic 3D structures by shining light on flat liquid crystalline vitrimer films without a mold. *J. Am. Chem. Soc.* **138**, 2118–2121 (2016).
19. Q. Shi *et al.*, Recyclable 3D printing of vitrimer epoxy. *Mater. Horiz.* **4**, 598–607 (2017).
20. M. M. Obadia, B. P. Mudraboyina, A. Serghei, D. Montarnal, E. Drockenmuller, Reprocessing and recycling of highly cross-linked ion-conducting networks through transalkylation exchanges of C-N bonds. *J. Am. Chem. Soc.* **137**, 6078–6083 (2015).
21. M. M. Obadia, A. Jourdain, P. Cassagnau, D. Montarnal, E. Drockenmuller, Tuning the viscosity profile of ionic vitrimers incorporating 1,2,3-triazolium cross-links. *Adv. Funct. Mater.* **27**, 1703258 (2017).
22. P. Chakma *et al.*, Anilinium salts in polymer networks for materials with mechanical stability and mild thermally induced dynamic properties. *ACS Macro Lett.* **8**, 95–100 (2019).
23. M. E. Belowich, J. F. Stoddart, Dynamic imine chemistry. *Chem. Soc. Rev.* **41**, 2003–2024 (2012).
24. M. Kathan *et al.*, Control of imine exchange kinetics with photoswitches to modulate self-healing in polysiloxane networks by light illumination. *Angew. Chem. Int. Ed. Engl.* **55**, 13882–13886 (2016).
25. X. Chen *et al.*, A thermally re-mendable cross-linked polymeric material. *Science* **295**, 1698–1702 (2002).
26. E. M. Foster *et al.*, Effect of polymer network architecture, enhancing soft materials using orthogonal dynamic bonds in an interpenetrating network. *ACS Macro Lett.* **6**, 495–499 (2017).
27. Y. Lai *et al.*, Colorless, transparent, robust, and fast scratch-self-healing elastomers via a phase-locked dynamic bonds design. *Adv. Mater.* **30**, e1802556 (2018).
28. A. Rekondo *et al.*, Catalyst-free room-temperature self-healing elastomers based on aromatic disulfide metathesis. *Mater. Horiz.* **1**, 237–240 (2014).
29. B. Zhang *et al.*, Probing the mechanism of thermally driven thiol-Michael dynamic covalent chemistry. *Org. Biomol. Chem.* **16**, 2725–2734 (2018).
30. M. D. Konieczynska *et al.*, On-demand dissolution of a dendritic hydrogel-based dressing for second-degree burn wounds through thiol-thioester exchange reaction. *Angew. Chem. Int. Ed. Engl.* **55**, 9984–9987 (2016).
31. D. Roy, J. N. Cambre, B. S. Sumerlin, Triply-responsive boronic acid block copolymers: Solution self-assembly induced by changes in temperature, pH, or sugar concentration. *Chem. Commun. (Camb.)* **16**, 2106–2108 (2009).
32. W. L. A. Brooks, B. S. Sumerlin, Synthesis and applications of boronic acid-containing polymers: From materials to medicine. *Chem. Rev.* **116**, 1375–1397 (2016).
33. R. C. Osthoff, A. M. Bueche, W. T. Grubb, Chemical stress-relaxation of polydimethylsiloxane elastomers1. *J. Am. Chem. Soc.* **76**, 4659–4663 (1954).
34. P. Zheng, T. J. McCarthy, A surprise from 1954: Siloxane equilibration is a simple, robust, and obvious polymer self-healing mechanism. *J. Am. Chem. Soc.* **134**, 2024–2027 (2012).
35. W.-P. Chen, D.-Z. Hao, W.-J. Hao, X.-L. Guo, L. Jiang, Hydrogel with ultrafast self-healing property both in air and underwater. *ACS Appl. Mater. Interfaces* **10**, 1258–1265 (2018).
36. A. P. Bapat, D. Roy, J. G. Ray, D. A. Savin, B. S. Sumerlin, Dynamic-covalent macromolecular stars with boronic ester linkages. *J. Am. Chem. Soc.* **133**, 19832–19838 (2011).
37. L. He, D. Szopinski, Y. Wu, G. A. Luinstra, P. Theato, Toward self-healing hydrogels using one-pot thiol-ene click and borax-diol chemistry. *ACS Macro Lett.* **4**, 673–678 (2015).
38. H. Meng *et al.*, pH- and sugar-induced shape memory hydrogel based on reversible phenylboronic acid-diol ester bonds. *Macromol. Rapid Commun.* **36**, 533–537 (2015).
39. D. Ailincai, G. Gavril, L. Marin, Polyvinyl alcohol boric acid - A promising tool for the development of sustained release drug delivery systems. *Mater. Sci. Eng. C* **107**, 110316 (2020).
40. C. Wang *et al.*, Recent advances in phenylboronic acid-based gels with potential for self-regulated drug delivery. *Molecules* **24**, 1089 (2019).
41. R. V. Gadhave, V. S. K, P. A. Mahanwar, P. T. Gadekar, Effect of addition of boric acid on thermo-mechanical properties of microcrystalline cellulose/polyvinyl alcohol blend and applicability as wood adhesive. *J. Adhes. Sci. Technol.* **35**, 1072–1086 (2021).
42. R. V. Gadhave, P. S. Kasbe, P. A. Mahanwar, P. T. Gadekar, To study the effect of boric acid modification on starch–polyvinyl alcohol blend wood adhesive. *J. Ind. Acad. Wood Sci.* **15**, 190–198 (2018).
43. T. G. Kane, "Polyvinyl alcohol adhesives containing boric acid and hexamethylenetetramine or triethylenediamine as additive to impart quick tack." US Patent US3320200A (1965).
44. H. Fan, J. P. Gong, Bioinspired underwater adhesives. *Adv. Mater.* **33**, e2102983 (2021).
45. K. L. Johnson, *Contact Mechanics* (Cambridge University Press, 1987).
46. H. Yuk *et al.*, Rapid and coagulation-independent haemostatic sealing by a paste inspired by barnacle glue. *Nat. Biomed. Eng.* **5**, 1131–1142 (2021).